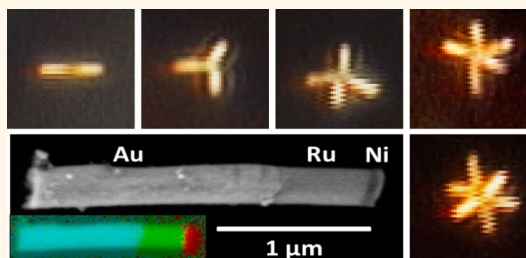


Self-Assembly of Nanorod Motors into Geometrically Regular Multimers and Their Propulsion by Ultrasound

Suzanne Ahmed,[†] Dillon T. Gentekos,[†] Craig A. Fink,[‡] and Thomas E. Mallouk^{*,†,§,||}

[†]Departments of Chemistry, [§]Physics, and ^{||}Biochemistry and Molecular Biology, The Pennsylvania State University, University Park, Pennsylvania 16802 United States and [‡]Philipsburg-Osceola Area High School, Philipsburg, Pennsylvania 16866, United States

ABSTRACT Segmented gold–ruthenium nanorods (300 ± 30 nm in diameter and 2.0 ± 0.2 μm in length) with thin Ni segments at one end assemble into few-particle, geometrically regular dimers, trimers, and higher multimers while levitated in water by ~ 4 MHz ultrasound at the midpoint of a cylindrical acoustic cell. The assembly of the nanorods into multimers is controlled by interactions between the ferromagnetic Ni segments. These assemblies are propelled autonomously in fluids by excitation with ~ 4 MHz ultrasound and exhibit several distinct modes of motion. Multimer assembly and disassembly are dynamic in the ultrasonic field. The relative numbers of monomers, dimers, trimers, and higher multimers are dependent upon the number density of particles in the fluid and their speed, which is in turn determined by the ultrasonic power applied. The magnetic binding energy of the multimers estimated from their speed-dependent equilibria is in agreement with the calculated strength of the magnetic dipole interactions. These autonomously propelled multimers can also be steered with an external magnetic field and remain intact after removal from the acoustic chamber for SEM imaging.



KEYWORDS: nanomotor · self-assembly · colloidal molecule · acoustic motor

The ability to controllably assemble materials with complex structures and properties from nanoscale building blocks is the focus of much current research.^{1–6} Controlled assembly of particles can yield colloid “molecules” with emergent properties that derive from their individual building blocks. Particles in such assemblies are also analogous to atoms in crystals, and imaging their interactions provides insight into microscopic phenomena such as crystal nucleation.^{7,8} Many kinds of interparticle interactions have been studied to control nanoparticle assembly. These include DNA base pairing,^{6,9,10} electrostatic,^{11–13} hydrophilic–hydrophobic,^{14,15} and magnetic interactions,^{16–28} as well as shape asymmetry.^{29–31}

In parallel, research into the collective interactions of powered microscale objects has been growing steadily and is of interest for understanding the emergent behavior of active matter.³² Most experimental studies of this kind have focused on living microorganisms or structurally simple objects such as polar nanorods, microspheres, or

irregularly shaped colloidal particles.^{33–42} Only a few studies have explored more complex designed shapes such as hinged nanorods⁴³ and self-assembled dimers and trimers.^{44–46} Deliberately assembled particles have the potential to exhibit different kinds of collective behavior and controllable movement and to incorporate several different kinds of materials and functions. Here we report the spontaneous assembly of acoustically levitated, dynamically propelled magnetic nanorods into geometrically regular “molecular” dimers, trimers, and higher multimers. The assembly and disassembly of these colloidal molecules occurs in water and in the absence of an applied magnetic field. In these experiments, ultrasonic acoustic power drives the rapid autonomous movement of individual nanorods and multimers. The kinetic energy imparted by ultrasonic excitation is important in the assembly/disassembly process because it can overcome the attractive energy of magnetic and surface interactions. Such interactions can otherwise dominate the assembly of nanoparticles,

* Address correspondence to tom.mallouk@gmail.com.

Received for review July 18, 2014 and accepted September 23, 2014.

Published online September 23, 2014
10.1021/nn5039614

© 2014 American Chemical Society

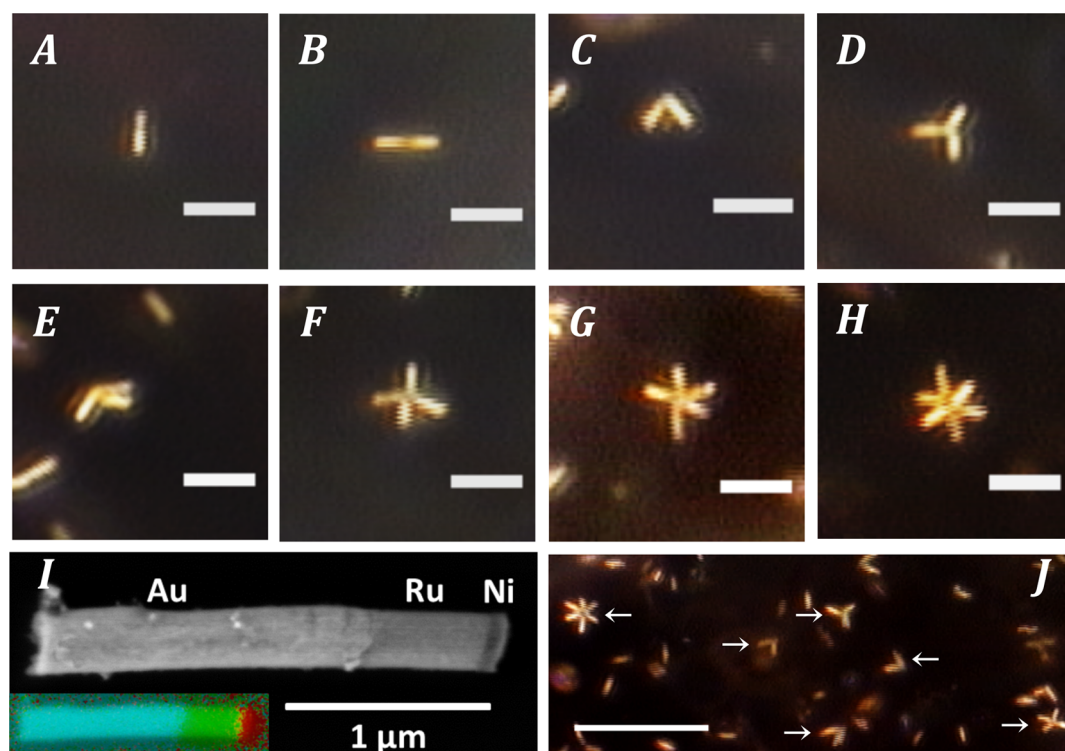


Figure 1. Nanorod monomers and multimers imaged in the levitation plane of an acoustic chamber. (a) Optical image of a monomer. (b) Linear dimer with magnetic segments touching face-to-face. (c) Bent dimer. (d) Trigonal planar trimer. (e) Trigonal pyramidal trimer. (f) Tetrahedral tetramer. (g) Trigonal bipyramidal pentamer. (h) Octahedral hexamer. (i) Field emission scanning electron micrograph (FE-SEM) image of a representative nanorod with an EDS inset with red, green, and blue false color representing Ni, Ru, and Au. (j) Lower magnification optical image of multimers in the levitation plane of the acoustic cell. Some multimers are pointed out with white arrows (density: $0.014 \text{ nanorods}/\mu\text{m}^2$, speed: $30 \mu\text{ms}^{-1}$). Scale bars for (a)–(h) are $5 \mu\text{m}$. Scale bar for (j) is $20 \mu\text{m}$. Figure S-2 and Video S-1 show additional low-magnification images and movies of multimers at low and high density of nanorods.

especially of highly polarizable metals, leading to irreversible aggregation and precipitation.

RESULTS AND DISCUSSION

Segmented Au–Ru–Ni rods were grown by sequential electrodeposition of metals in porous anodic alumina templates from commercial plating solutions as previously described.⁴⁷ The rods were $300 \pm 30 \text{ nm}$ in diameter and $2.0 \pm 0.3 \mu\text{m}$ in length. The Ni, Au, and Ru segments were respectively $80 \pm 20 \text{ nm}$, $1.4 \pm 0.2 \mu\text{m}$, and $0.55 \pm 0.09 \mu\text{m}$ in length.

The nanorods were placed in a cylindrical acoustic chamber, $180 \pm 10 \mu\text{m}$ height, $5.0 \pm 0.1 \text{ mm}$ diameter, as previously described.⁴⁸ A schematic of the experimental setup is shown in Figure S1. Upon excitation at the resonant frequency of the cell ($\sim 4 \text{ MHz}$), the rods levitated to the midplane underwent the behaviors previously observed with nonmagnetic metallic rods: autonomous axial propulsion and formation of spinning chains and concentric circles of rods at the lateral acoustic nodes. The autonomous axial motion within the levitation plane derives from acoustically driven fluid streaming around the dense metal rods, which are axially asymmetric because of their concave and convex ends.⁴⁹ Unlike nanorod motors that contained

magnetic stripes in the center of the rods, those with Ni stripes at the ends spontaneously assembled into dimers, trimers, and higher multimers depending on the density of the rod suspensions and the speed of their axial movement within the levitation plane.

Interestingly, the rods tended to assemble into regular “molecular” geometries, as shown in Figure 1. Earlier experiments have shown that thin Ni segments in Au–Pt nanorods of similar dimensions to those studied here tend to be single-domain ferromagnets, in which the magnetic dipole is oriented in the plane of the Ni disk.⁴⁷ The formation of a linear head-to-head dimer from two Ni-tipped rods can be understood as the minimization of magnetic energy through the interaction of these dipoles. We show below that this energy is on the order of 10^{-17} J for the assembly of dimers. The formation of regular multimers also clearly results from magnetic interactions, which are the strongest forces in the system, but the details of the orientation and arrangement of magnetic dipoles are not yet understood.

These assemblies are propelled in the acoustic field and exhibit different modes of motion. As they are propelled in the fluid, drag forces tend to break the

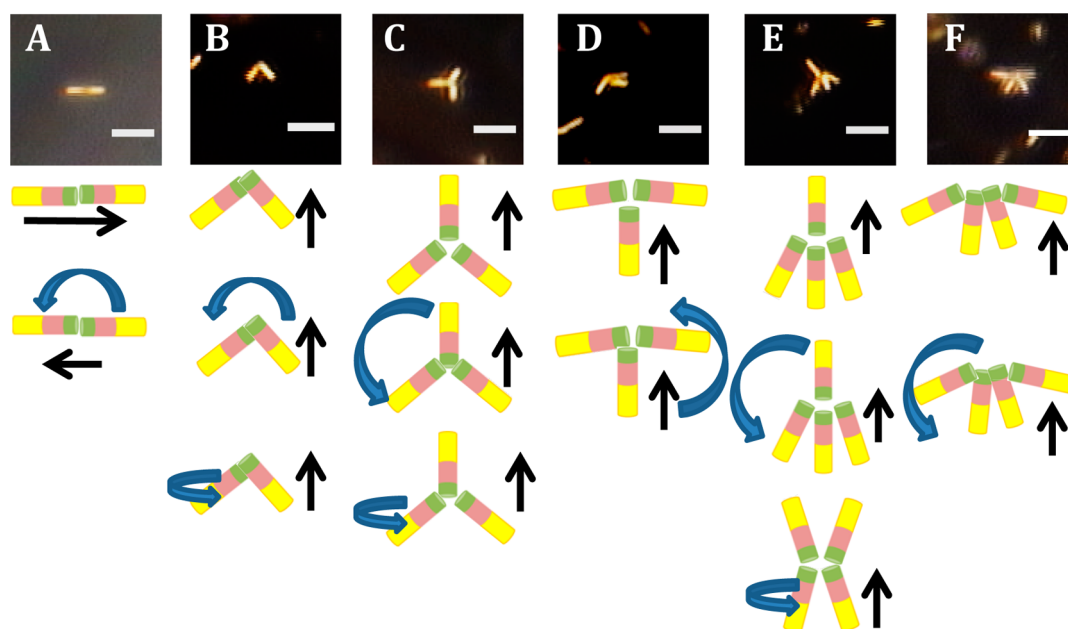


Figure 2. Optical micrographs and schematic drawings of the most common modes of motion of dimers, trimers, and tetramers. (A) Linear dimer: (top) one gold end leading, (bottom) rotating while translating. (B) Bent dimer: (top) nickel ends leading, (middle) rotating while translating, (bottom) spinning while translating in a nodal line. (C) Trigonal planar trimer: (top) a gold end leading, (middle) rotating while translating, (bottom) base spinning relative to leading wire of structure. (D) Pyramidal/T-shaped trimer: (top) nickel ends leading, (bottom) rotating while translating with nickel ends leading. (E) Tetrahedral tetramer: (top) a gold end leading, (middle) rotating while translating, (bottom) in a nodal line in an X-shaped structure with its two-wire base rotating with respect to its two-wire top. (F) Square pyramidal tetramer: (top) nickel ends leading, (bottom) rotating while translating nickel ends leading. The scale bars are $5\ \mu\text{m}$. Black arrows indicate translational motion, and blue arrows represent rotations. These modes are illustrated in Video S-2.

symmetry of the multimers with the magnetic segments serving as flexible hinges, as shown in Figure 2.

Modes of Motion. Various modes of motion were observed for the monomers and multimers. Monomers exhibit axial autonomous motion with the nickel end leading. Dimers move in a linear conformation with the gold segment of one of the component rods leading or in a bent conformation with the nickel segments leading. The direction of movement in the bent conformation is consistent with the nickel end leading in the axial propulsion of rod monomers. Trimers have several modes of movement: translation as a trigonal planar structure with one gold end leading, translation with the nickel segments leading in a trigonal pyramidal or T-shaped conformation, in-plane rotation of the complete trigonal planar or trigonal pyramidal structure, and out-of-plane rotation of the base of the trigonal plane. The latter mode is typically observed within nodal lines. Tetramers tend to translate axially with the gold end of one of its component nanorods leading, as a square pyramid with the nickel segments leading, or *via* rotation of the square pyramidal structure. Within the acoustic nodal lines of the cell, tetramers form an X-shaped conformation with its two-wire base rotating with respect to its two-wire top. Pentamers and larger assemblies tend to translate axially as a whole or rotate as a whole. The most prevalent modes of motion are sketched in Figure 2 and can be seen in Video S-2.

Dynamic Equilibrium: Assembly and Disassembly of Multimers. The assembly of multimers tends to occur through bimolecular collisions. This can occur as a result of the collision of two monomers, a dimer and a monomer, a monomer and a trimer, or two multimers, to form a larger assembly. Disassembly occurs spontaneously (presumably when the instantaneous shear force exceeds the magnetic attraction between the component nanorods) or as a result of a collision with another motor that causes fragmentation. Frame sequences of some examples of assembly and disassembly can be seen in Figure 3 and Video S-3. The relative numbers of monomers, dimers, trimers, and higher multimers are dependent upon the number density of particles in the fluid and the speed of the motors, which is determined by the ultrasonic power applied. Hence a dynamic equilibrium is established between multimers, and the system can be modeled as a set of stepwise association reactions with equilibrium constants for each. The propulsion force is analogous to thermal excitation, and thus the equilibrium constants depend on motor speed.

Expressions for the system of equilibria (1–5) were derived (see Supporting Information), and the number density of multimers at varying total concentrations of rods was measured at three different speeds (as determined from the average speeds of the monomers).

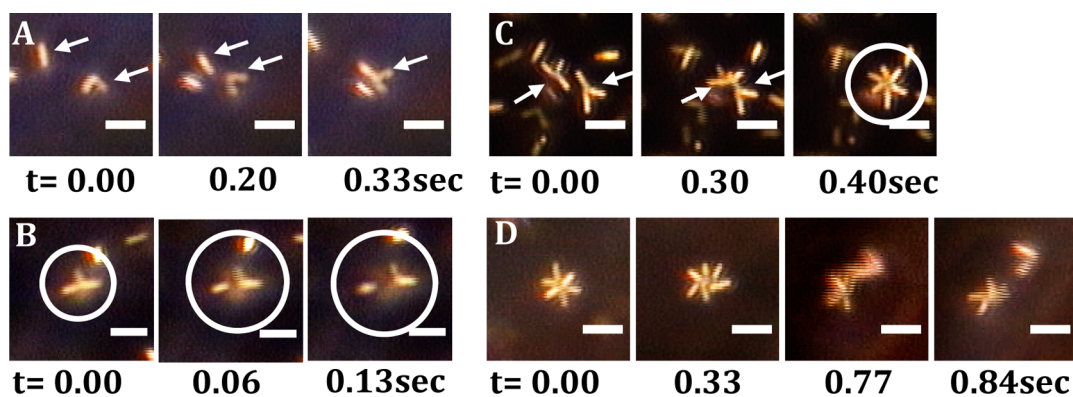
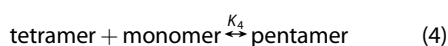
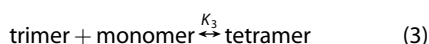
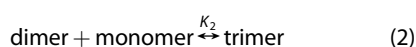


Figure 3. Representative assembly and disassembly frame sequences of nanorod multimers. (A) Assembly of a trimer from a monomer and a dimer. (B) Disassembly of a trimer into a monomer and a dimer. (C) Assembly of a hexamer from two trimers. (D) Disassembly of a hexamer. White arrows and circles indicate motors involved. Scale bars are $5 \mu\text{m}$.

TABLE 1. Equilibrium Constants (μm^2) for Dimer and Trimer (Reactions 1 and 2) at Three Different Monomer Speeds, with Standard Deviations Indicated in Parentheses

speed ($\mu\text{m s}^{-1}$)	K_1	K_2
17 (5)	36 (13)	63 (22)
30 (7)	16 (6)	50 (16)
55 (8)	13 (6)	38 (11)



At a given speed, equilibrium constants K_1 and K_2 and their standard deviations (Table 1) could be obtained from global fits of the measured densities of monomers, dimers, and trimers (Figure 4).

Because the ultrasonic standing wave confines the nanorods within a largely 2D levitation plane, the number density of monomers and multimers was measured per unit area (as opposed to per unit volume). At low concentration, as the number density of rods in the levitation plane increases, so does the number of monomers. The monomer concentration initially increases linearly with total rod density and then grows more slowly as dimers and higher multimers begin to form (Figure 4).

The equilibrium distribution of multimers is dependent on the speed of particles, which provides a kind of thermal excitation that balances the attractive magnetic interaction between the ferromagnetic nickel segments. As the speed increases, the distribution shifts toward monomers, consistent with the idea that the association into multimers is exothermic. Pentamers and hexamers appear at lower speeds, and multimers higher than trimers are not present at all at

the highest speed sampled in these experiments ($55 \mu\text{m s}^{-1}$). Equilibrium constants for the dimer and trimer assembly reactions at the three speeds tested are given in Table 1.

The assembly energy is the attractive magnetic energy of association of the nickel segments of the monomers, plus smaller contributions from van der Waals attractive and electrostatic repulsive energies between the negatively charged rods. A previous study of chemically powered nanorod assembly has established that the van der Waals and electrostatic energies are small compared to the Brownian (thermal) energy in the absence of fuel.⁴⁵ The magnetic energy between the magnetic dipole of two rods suspended in water can be calculated as⁵⁰

$$E_m = \frac{\mu m_1 m_2 \cos(\theta)}{4\pi r^3} \quad (6)$$

where E_m is the magnetic potential energy, μ is the permittivity of water ($1.26 \times 10^{-6} \text{ N A}^{-2}$), and m_1 and m_2 are the magnetic dipole moment of the rods, which was determined to be $(2.0 \pm 0.5) \times 10^{-15} \text{ A} \cdot \text{m}^2$ at 298 K by using SQUID magnetometry. The distance between the magnetic dipoles at the ends of the rods is r . For dimers moving at $30 \mu\text{m s}^{-1}$, the most common shape was a "V" with an angle θ of approximately 100° . The distance r was taken as $0.15 \mu\text{m}$, which is the center-to-center distance of the magnetic stripes in this geometry. From eq 6, we thus obtain $E_m = (2.0 \pm 0.5) \times 10^{-17} \text{ J}$.

Because propulsion provides a kind of thermal or kinetic energy that causes dissociation of dimers and higher multimers, the ratio of the magnetic energy E_m to the propulsion energy E_p can be estimated from the rate of dissociation using the Arrhenius equation

$$k = A \exp\left(-\frac{E_m}{E_p}\right) \quad (7)$$

The experimental dissociation rate constants were determined for dimers and trimers moving at speeds of 17, 30, and $55 \mu\text{m s}^{-1}$ to be 0.08, 0.2, and 0.5 s^{-1} , respectively,

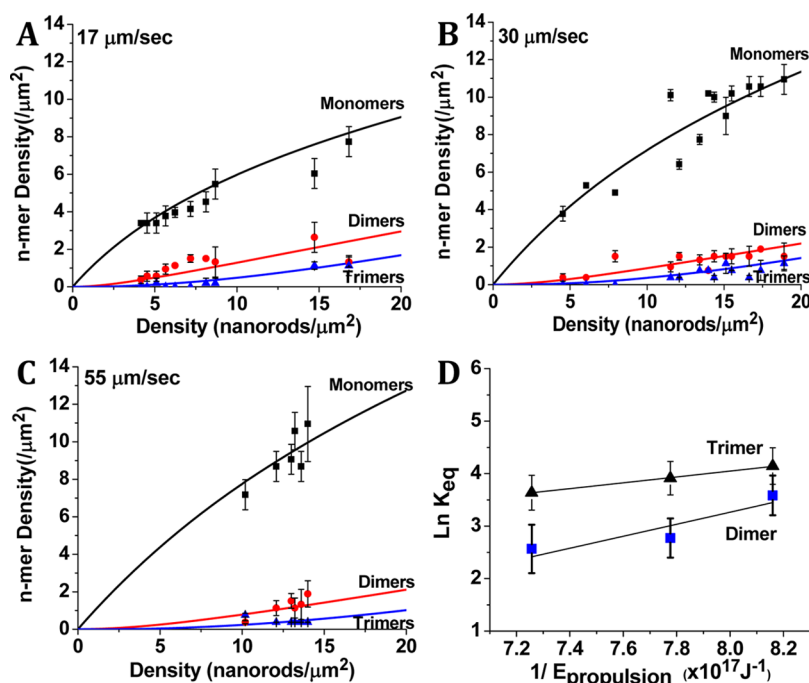


Figure 4. Multimer density as a function of number density of particles in solution at different average monomer speeds. Expressions derived for the equilibrium concentrations of monomers, dimers, and trimers (see SI) were used to fit the experimental data points. Fit lines are drawn for monomers, dimers, and trimers, at (A) 17 ± 5 , (B) 30 ± 8 , and (C) $55 \pm 7 \mu\text{m s}^{-1}$. (D) van't Hoff plot of the propulsion energy dependence of the equilibrium constants of dimers and trimers.

with corresponding persistence times of 13, 6, and 2 s. We can estimate the attempt frequency A using $A = f/2m$, where $f = F_{\text{drag}}/v$, where F_{drag} is the drag force, v is the velocity, and m is the mass of the rod.⁵¹ The drag force F_{drag} on a cylinder moving at axial velocity v is given by⁵²

$$F_{\text{drag}} = \frac{2\pi\eta L}{\ln\left(\frac{L}{R}\right) - 0.72} v \quad (8)$$

where L is the length of the rod ($2.0 \mu\text{m}$), R is its radius ($0.30 \mu\text{m}$), and η is the kinematic viscosity of the water ($1.0 \times 10^{-3} \text{ Pa}\cdot\text{s}$). From this calculation we obtain $A = 1.4 \times 10^6 \text{ s}^{-1}$. Using the E_m value calculated above, we then obtain propulsion energies E_p of 1.2, 1.3, and $1.4 \times 10^{-18} \text{ J}$ from eq 7 for wires traveling at 17, 30, and $55 \mu\text{m s}^{-1}$, respectively. Note that this simple calculation ignores the electrostatic and van der Waals components of the interaction energy between rods, which are expected to be small compared to E_m .

Using the values of E_p derived from the Arrhenius equation, we can extract monomer–monomer and dimer–monomer binding energies from the velocity dependence of the equilibrium constant. The van't Hoff equation relates the temperature dependence of the equilibrium constant to the reaction enthalpy:

$$\ln K_{\text{eq}} = -\frac{\Delta H}{k_B T} + \frac{\Delta S}{k_B} \quad (9)$$

Here k_B is Boltzmann's constant and T is the system temperature. Because propulsion provides an average

kinetic energy that causes dissociation, we can substitute E_p for $k_B T$, yielding

$$\ln K_{\text{eq}} = -\frac{\Delta H}{E_p} + \frac{\Delta S}{k_B} \quad (10)$$

Thus, a van't Hoff plot (Figure 4d) should have a slope of $-\Delta H$, from which we can calculate a dimer dissociation energy of $1.1 \times 10^{-17} \text{ J}$. This value is in reasonable agreement with the calculated magnetic binding energy ($E_m = 2.0 \times 10^{-17} \text{ J}$) and adds further support to the equilibrium model. From the equilibrium data (Figure 4) and the van't Hoff equation, we can also estimate an energy for the formation of a trimer. An additional stability of $0.6 \times 10^{-17} \text{ J}$ is gained by forming a trimer from a monomer and a dimer.

We can gain further insight into the balance of forces operating in the system by noting that the propulsion force equals the drag force at low Reynolds number and is directly proportional to the velocity of the rods (eq 8). F_{drag} for monomers moving axially at 17, 30, and $55 \mu\text{m s}^{-1}$ is 1.1, 2.0, and $3.7 \times 10^{-13} \text{ N}$, respectively. When aggregates of rods dissociate spontaneously, this force must be comparable to the attractive force between their components. The magnetic component of the attractive force between rods can be obtained by differentiating eq 6 to yield eq 11:

$$F_m = -\frac{3\mu m_1 m_2}{4\pi r^4} \quad (11)$$

This force is equal to F_{drag} at r values of 1.8, 1.6, and $1.3 \mu\text{m}$ for speeds of 17, 30, and $55 \mu\text{m s}^{-1}$, respectively. This is

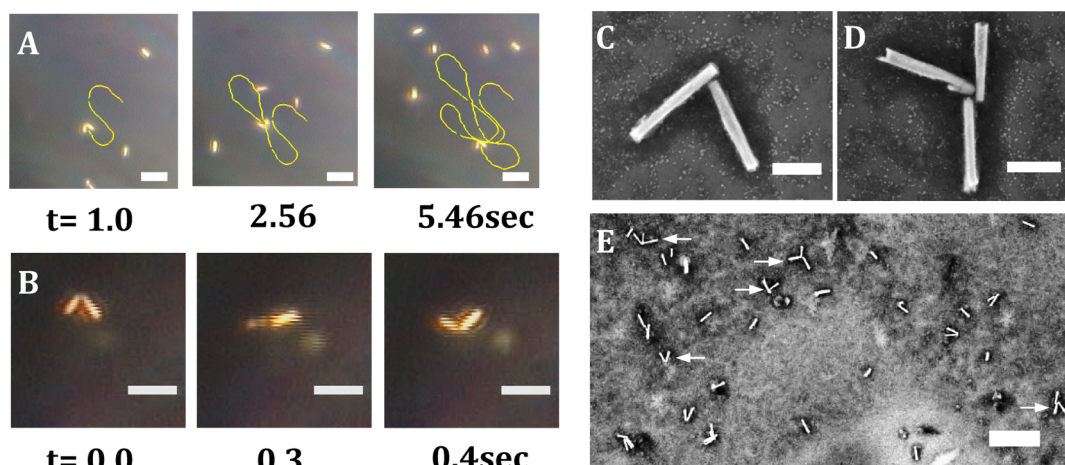


Figure 5. Magnetic steering, manipulation, and isolation of assemblies. (A) Optical image frame sequence of the deliberate steering of a dimer through sharp loops using an external magnetic field. Time stamps are indicated, and tracking is shown as a yellow line. Scale bar is $10\ \mu\text{m}$. (B) Optical image frame sequence for magnetic manipulation of the mode of motion of a dimer. The dimer is made to go through full inversions as it propels. Scale bar is $5\ \mu\text{m}$. (C, D) SEM images of a dimer (C) and trimer (D) pipetted out of the acoustic cell and dried on a conductive Si wafer. Scale bars are $1\ \mu\text{m}$. These assemblies are pointed out with white arrows in lower magnification SEM image (E), scale bar $10\ \mu\text{m}$.

consistent with our observations that rods passing within $1\text{--}2\ \mu\text{m}$ of each other can be “captured” to form aggregates. Rods passing within this distance of aggregates can also impart sufficient force to dissociate the aggregates. An example of such a “fly-by”-induced dissociation can be seen in Figure S-3 and corresponding Video S-4.

Magnetic Manipulation. Magnetic manipulation of colloidal asters has previously been studied, although in much larger (millimeter-scale) assemblies.⁵³ Here we conduct some simple experiments to show that nanorod multimers, like monomers containing magnetic stripes that we reported previously, can be steered in magnetic fields while remaining intact. Using the experimental setup we previously reported,⁵⁴ a weak magnetic field (on the order of $45\ \text{mT}$) was applied using hand-held Nd–Fe–B magnets. The magnets were held in the plane of the acoustic cell at a distance of about $2.5\ \text{cm}$ from the sample under observation. The assemblies were reoriented by the magnet and steered to make several loops, as shown in Figure 5a. Steering of multimers can be seen in Video S-5.

Interestingly the mode of motion of an n -mer can also be altered by using a magnetic field. This is because the magnetic components behave as flexible hinges, which can allow a variety of motions. A dimer, with application of an external magnetic field, can be driven to make several complete inversions in a “flapping” motion while being acoustically propelled in one direction. This is illustrated in Figure 5b and Video S-6.

MATERIALS AND METHODS

Nanowire Synthesis and Characterization. Nanowires were grown by electrodeposition within the pores of commercial anodic alumina templates (Whatman Inc., nominal pore size $0.2\ \mu\text{m}$,

ISOLATION AND IMAGING

Once assembled in water, the rod multimers can be isolated by drying, as shown in Figure 5. The nanorod suspension in the acoustic chamber was pipetted out, placed on a conductive silicon wafer, and dried for FE-SEM imaging. These images show that the colloidal “molecules” remain largely intact, but are flattened by capillary forces and surface interactions in the drying process. It remains to be seen if suspensions of regular multimers can be reconstituted from dried samples deposited on appropriate substrates.

CONCLUSION

Metal nanorods tipped with ferromagnetic segments assemble into n -mer “molecules” with regular geometries while levitated in a fluid acoustic cell. Levitation with ultrasound allows us to eliminate surface effects and sedimentation, enabling assembly in the absence of an applied magnetic field and in an ordinary fluid (water). The relative concentrations of multimers are described by a set of stepwise equilibrium constants, and the kinetics of their dissociation obey the Arrhenius law, both of which are modulated by an effective temperature that is controlled by adjusting the acoustic power. These assemblies are dynamic motors that exhibit various modes of motion. They can be steered with a weak applied magnetic field, their modes of motion can be altered by the magnetic field, and they can be isolated while remaining intact.

actual pore diameter $\sim 0.3\ \mu\text{m}$). Au, Ru, and Ni segments were grown sequentially by changing the deposition solution and electroplating conditions. Commercial electroplating solutions (Technic Inc., Au-Orotemp 24 RTU, Ru–U solution and Ni–Nickel

Sulfamate RTU) were used. Gold and nickel were deposited at constant cathodic current densities of 1.17 and 0.7 mA/cm², for 15 and 6 min, respectively. A layer of evaporated silver on the porous anodic alumina membrane served as the cathode, and a Pt wire was used as the anode. Ruthenium was deposited for 30 min at a constant potential of -0.65 V vs a Ag/AgCl reference electrode.

The magnetic properties of nanowires were characterized using a SQUID magnetometer from Quantum Design, Inc. Scanning electron microscopy (SEM) images were collected with an FEI Nova NanoSEM 630 FESEM with EDS. A backscatter detector and beam deceleration were used to obtain high elemental contrast images shown in Figure 1.

Acoustic Experiments. Acoustic propulsion experiments were carried out in an acoustic chamber previously described⁴⁸ and shown schematically in Figure S-1. The chamber was constructed of a stainless steel plate (4.2 cm × 4.2 cm × 1 mm) with a circular piezoelectric transducer attached to it (1 mm thickness) on one side and several layers of Kapton tape (height 180 ± 10 μm) on the other side. A 5.0 ± 0.1 mm diameter hole was punched into the Kapton tape to define the cell. A glass coverslip was placed on top of the cell and served as a reflector to set up a standing acoustic wave that levitated and propelled the wires. The piezoelectric was actuated at ~ 4 MHz using a 10 V peak-to-peak signal from a waveform generator. Videos and images were collected 2–3 min after the acoustic power was turned on in order to ensure an equilibrium distribution of multimers.

Optical Imaging and Tracking. Videos were recorded using an Olympus BX60 microscope at 500× magnification at a frame rate of 30 s⁻¹ using the video software Dazzle Video Creator Plus. Nanowire tracking was carried out using the open access Video Spot Tracker software (http://cisimm.cs.unc.edu/downloads/?dl_cat=3).

Conflict of Interest: The authors declare no competing financial interest.

Acknowledgment. We thank Darrell Velegol for helpful discussions, Nitin Samarth and Robbie Fraleigh for assistance with the SQUID magnetometer, and Trevor Clark for assistance with FE-SEM imaging and EDS. This work was supported by the National Science Foundation under MRSEC grant DMR-0820404. C.A.F. acknowledges support from the National Science Foundation Research Experiences for Teachers program, DMR-1125591. Analytical instrumentation used in this work was supported by the Pennsylvania State University Materials Research Institute Nanofabrication Laboratory under National Science Foundation Cooperative Agreement ECS-0335765.

Supporting Information Available: Schematic drawings of the acoustic sample cell, optical microscope images and videos of nanorod monomers and multimers at high and low density, images and videos of assembly and disassembly of multimers, and description of videos. This material is available free of charge via the Internet at <http://pubs.acs.org>.

REFERENCES AND NOTES

- Whitesides, G. M.; Grzybowski, B. Self-Assembly at All Scales. *Science* **2002**, *295*, 2418–2421.
- Li, F.; Josephson, D. P.; Stein, A. Colloidal Assembly: The Road from Particles to Colloidal Molecules and Crystals. *Angew. Chem., Int. Ed.* **2011**, *50*, 360–388.
- Löwen, H. Colloidal Dispersions in External Fields: Recent Developments. *J. Phys.: Condens. Matter* **2008**, *20*, 404201.
- Shevchenko, E. V.; Talapin, D. V.; Kotov, N. A.; O'Brien, S.; Murray, C. B. Structural Diversity in Binary Nanoparticle Superlattices. *Nature* **2006**, *439*, 55–59.
- Damasceno, P. F.; Engel, M.; Glotzer, S. C. Predictive Self-Assembly of Polyhedra into Complex Structures. *Science* **2012**, *337*, 453–457.
- Grzybowski, B.; Jiang, X.; Stone, H.; Whitesides, G. Dynamic, Self-Assembled Aggregates of Magnetized, Millimeter-Sized Objects Rotating at the Liquid-Air Interface:

- Macroscopic, Two-Dimensional Classical Artificial Atoms and Molecules. *Phys. Rev. E* **2001**, *64*, 011603.
- Schade, N. B.; Holmes-Cerfon, M. C.; Chen, E. R.; Aronson, D.; Collins, J. W.; Fan, J. A.; Capasso, F.; Manoharan, V. N. Tetrahedral Colloidal Clusters from Random Packing of Bidisperse Spheres. *Phys. Rev. Lett.* **2013**, *110*, 148303.
 - Arkus, N.; Manoharan, V.; Brenner, M. Minimal Energy Clusters of Hard Spheres with Short Range Attractions. *Phys. Rev. Lett.* **2009**, *103*, 118303.
 - Mastroianni, A. J.; Claridge, S. A.; Alivisatos, A. P. Pyramidal and Chiral Groupings of Gold Nanocrystals Assembled Using DNA Scaffolds. *J. Am. Chem. Soc.* **2009**, *131*, 8455–8459.
 - Xu, X.; Rosi, N. L.; Wang, Y.; Huo, F.; Mirkin, C. A. Asymmetric Functionalization of Gold Nanoparticles with Oligonucleotides. *J. Am. Chem. Soc.* **2006**, *128*, 9286–9287.
 - Gangwal, S.; Cayre, O. J.; Velev, O. D. Dielectrophoretic Assembly of Metallodielectric Janus Particles in AC Electric Fields. *Langmuir* **2008**, *24*, 13312–13320.
 - Ma, F.; Wu, D. T.; Wu, N. Formation of Colloidal Molecules Induced by Alternating-Current Electric Fields. *J. Am. Chem. Soc.* **2013**, *135*, 7839–7842.
 - Chaudhary, K.; Chen, Q.; Juárez, J. J.; Granick, S.; Lewis, J. A. Janus Colloidal Matchsticks. *J. Am. Chem. Soc.* **2012**, *134*, 12901–12903.
 - Chen, Q.; Bae, S. C.; Granick, S. Directed Self-Assembly of a Colloidal Kagome Lattice. *Nature* **2011**, *469*, 381–384.
 - Gao, W.; Pei, A.; Feng, X.; Hennessy, C.; Wang, J. Organized Self-Assembly of Janus Micromotors with Hydrophobic Hemispheres. *J. Am. Chem. Soc.* **2013**, *135*, 998–1001.
 - Yan, J.; Chaudhary, K.; Chul Bae, S.; Lewis, J. A.; Granick, S. Colloidal Ribbons and Rings from Janus Magnetic Rods. *Nat. Commun.* **2013**, *4*, 1516.
 - Erb, R. M.; Son, H. S.; Samanta, B.; Rotello, V. M.; Yellen, B. B. Magnetic Assembly of Colloidal Superstructures with Multipole Symmetry. *Nature* **2009**, *457*, 999–1002.
 - Goubault, C.; Leal-Calderon, F.; Viovy, J.-L.; Bibette, J. Self-Assembled Magnetic Nanowires Made Irreversible by Polymer Bridging. *Langmuir* **2005**, *21*, 3725–3729.
 - Helseth, L. E. Self-assembly of Colloidal Pyramids in Magnetic Fields. *Langmuir* **2005**, *21*, 7276–7279.
 - Ilievski, F.; Mani, M.; Whitesides, G. M.; Brenner, M. P. Self-Assembly of Magnetically Interacting Cubes by a Turbulent Fluid Flow. *Phys. Rev. E* **2011**, *83*, 017301.
 - Martínez Pedrero, F.; Tirado Miranda, M.; Schmitt, A.; Callejas Fernández, J. Forming Chainlike Filaments of Magnetic Colloids: The Role of the Relative Strength of Isotropic and Anisotropic Particle Interactions. *J. Chem. Phys.* **2006**, *125*, 084706.
 - Ooi, C.; Erb, R. M.; Yellen, B. B. On the Controllability of Nanorod Alignment in Magnetic Fluids. *J. Appl. Phys.* **2008**, *103*, 07E910.
 - Piet, D. L.; Straube, A. V.; Snezhko, A.; Aranson, I. S. Viscosity Control of the Dynamic Self-Assembly in Ferromagnetic Suspensions. *Phys. Rev. Lett.* **2013**, *110*, 198001.
 - Rybczynski, J.; Ebels, U.; Giersig, M. Large-Scale, 2D Arrays of Magnetic Nanoparticles. *Colloids Surf., A* **2003**, *219*, 1–6.
 - Smoukov, S. K.; Gangwal, S.; Marquez, M.; Velev, O. D. Reconfigurable Responsive Structures Assembled from Magnetic Janus Particles. *Soft Matter* **2009**, *5*, 1285.
 - Snezhko, A.; Aranson, I.; Kwok, W.-K. Dynamic Self-Assembly of Magnetic Particles on the Fluid Interface: Surface-Wave-Mediated Effective Magnetic Exchange. *Phys. Rev. E* **2006**, *73*, 041306.
 - Yang, Y.; Gao, L.; Lopez, G. P.; Yellen, B. B. Tunable Assembly of Colloidal Crystal Alloys Using Magnetic Nanoparticle Fluids. *ACS Nano* **2013**, *7*, 2705–2716.
 - Piet, D. L.; Straube, A. V.; Snezhko, A.; Aranson, I. S. Model of Dynamic Self-Assembly in Ferromagnetic Suspensions at Liquid Interfaces. *Phys. Rev. E* **2013**, *88*, 033024.
 - Sacanna, S.; Irvine, W. T. M.; Chaikin, P. M.; Pine, D. J. Lock and Key Colloids. *Nature* **2010**, *464*, 575–578.
 - Walker, D. A.; Leitsch, E. K.; Nap, R. J.; Szleifer, I.; Grzybowski, B. A. Geometric Curvature Controls the Chemical Patchiness and Self-Assembly of Nanoparticles. *Nat. Nanotechnol.* **2013**, *8*, 676–681.

31. Velev, O. D. Patchy Nanoparticles: Curvature Makes a Difference. *Nat. Nanotechnol.* **2013**, *8*, 620–621.
32. Marchetti, M. C.; Joanny, J. F.; Ramaswamy, S.; Liverpool, T. B.; Prost, J.; Rao, M.; Simha, R. A. Hydrodynamics of Soft Active Matter. *Rev. Mod. Phys.* **2013**, *85*, 1143–1189.
33. Surrey, T.; Nedelec, F.; Leibler, S.; Karsenti, E. Physical Properties Determining Self-Organization of Motors and Microtubules. *Science* **2001**, *292*, 1167–1171.
34. Ibele, M.; Mallouk, T. E.; Sen, A. Schooling Behavior of Light-Powered Autonomous Micromotors in Water. *Angew. Chem., Int. Ed.* **2009**, *48*, 3308–3312.
35. Dombrowski, C.; Cisneros, L.; Chatkaew, S.; Goldstein, R. E.; Kessler, J. O. Self-Concentration and Large-Scale Coherence in Bacterial Dynamics. *Phys. Rev. Lett.* **2004**, *93*, 098103.
36. Bendix, P. M.; Koenderink, G. H.; Cuvelier, D.; Dogic, Z.; Koелеman, B. N.; Brierher, W. M.; Field, C. M.; Mahadevan, L.; Weitz, D. a A Quantitative Analysis of Contractility in Active Cytoskeletal Protein Networks. *J. Biophys.* **2008**, *94*, 3126–3136.
37. Wilson, D. A.; Nolte, R. J. M.; Van Hest, J. C. M. Autonomous Movement of Platinum-Loaded Stomatocytes. *Nat. Chem.* **2012**, *4*, 268–274.
38. Cates, M. E.; Marenduzzo, D.; Pagonabarraga, I.; Tailleur, J. Arrested Phase Separation in Reproducing Bacteria Creates a Generic Route to Pattern Formation. *Proc. Natl. Acad. U.S.A.* **2010**, *107*, 11715–11720.
39. Kagan, D.; Balasubramanian, S.; Wang, J. Chemically Triggered Swarming of Gold Microparticles. *Angew. Chem., Int. Ed.* **2011**, *50*, 503–506.
40. Miño, G.; Mallouk, T. E.; Darnige, T.; Hoyos, M.; Dauchet, J.; Dunstan, J.; Soto, R.; Wang, Y.; Rousselet, A.; Clement, E. Enhanced Diffusion Due to Active Swimmers at a Solid Surface. *Phys. Rev. Lett.* **2011**, *106*, 048102.
41. Palacci, J.; Sacanna, S.; Steinberg, A. P.; Pine, D. J.; Chaikin, P. M. Living Crystals of Light-Activated Colloidal Surfers. *Science* **2013**, *339*, 936–940.
42. Saintillan, D.; Shelley, M. J. Active Suspensions and Their Nonlinear Models. *C. R. Phys.* **2013**, *14*, 497–517.
43. Gao, W.; Sattayasamitsathit, S.; Manesh, K. M.; Weihs, D.; Wang, J. Magnetically Powered Flexible Metal Nanowire Motors. *J. Am. Chem. Soc.* **2010**, *132*, 14403–14405.
44. Gibbs, J. G.; Zhao, Y. Self-Organized Multiconstituent Catalytic Nanomotors. *Small* **2010**, *6*, 1656–1662.
45. Wang, W.; Duan, W.; Sen, A.; Mallouk, T. E. Catalytically Powered Dynamic Assembly of Rod-Shaped Nanomotors and Passive Tracer Particles. *Proc. Natl. Acad. U.S.A.* **2013**, *110*, 17744–17749.
46. Dong, B.; Zhou, T.; Zhang, H.; Li, C. Y. Directed Self-Assembly of Nanoparticles for Nanomotors. *ACS Nano* **2013**, *7*, 5192–5198.
47. Kline, T. R.; Tian, M.; Wang, J.; Sen, A.; Chan, M. W. H.; Mallouk, T. E. Template-Grown Metal Nanowires. *Inorg. Chem.* **2006**, *45*, 7555–7565.
48. Wang, W.; Castro, L. A.; Hoyos, M.; Mallouk, T. E. Autonomous Motion of Metallic Microrods Propelled by Ultrasound. *ACS Nano* **2012**, *6*, 6122–6132.
49. Nadal, F.; Lauga, E. Asymmetric Steady Streaming as a Mechanism for Acoustic Propulsion of Rigid Bodies. *Phys. Fluids* **2014**, *26*, 082001.
50. Khalil, K. S.; Sagastegui, A.; Li, Y.; Tahir, M. A.; Socolar, J. E. S.; Wiley, B. J.; Yellen, B. B. Binary Colloidal Structures Assembled through Ising Interactions. *Nat. Commun.* **2012**, *3*, 794.
51. Li, T.; Kheifets, S.; Medellin, D.; Raizen, M. G. Measurement of the Instantaneous Velocity of a Brownian Particle. *Science* **2010**, *328*, 1673–1675.
52. Happel, J.; Brenner, H. *Low Reynolds Number Hydrodyn.* **1965**, 229.
53. Snezhko, A.; Aranson, I. S. Magnetic Manipulation of Self-Assembled Colloidal Asters. *Nat. Mater.* **2011**, *10*, 698–703.
54. Ahmed, S.; Wang, W.; Mair, L. O.; Fraleigh, R. D.; Li, S.; Castro, L. A.; Hoyos, M.; Huang, T. J.; Mallouk, T. E. Steering Acoustically Propelled Nanowire Motors toward Cells in a Biologically Compatible Environment Using Magnetic Fields. *Langmuir* **2013**, *29*, 16113–16118.